

**Rephasing of optically driven atomic coherences by rapid adiabatic passage in  $\text{Pr}^{3+}:\text{Y}_2\text{SiO}_5$** 

Simon Mieth,\* Daniel Schraft, and Thomas Halfmann

*Institut für Angewandte Physik, Technische Universität Darmstadt, Hochschulstrasse 6, 64289 Darmstadt, Germany*

Leonid P. Yatsenko

*Institute of Physics, National Academy of Sciences of Ukraine, prospect Nauki 46, Kiev-39, 03650, Ukraine*

(Received 5 April 2012; revised manuscript received 17 October 2012; published 6 December 2012)

We present experimental investigations of rephasing optically driven atomic coherences, prepared by electromagnetically induced transparency in a  $\text{Pr}^{3+}:\text{Y}_2\text{SiO}_5$  crystal. In particular, we systematically study rephasing based on rapid adiabatic passage and compare the performance of the latter with standard rephasing based on Hahn spin echoes. The data clearly demonstrate the superior performance of rapid adiabatic passage for any application of rephasing, which suffers from large inhomogeneous broadenings in the medium or inevitable fluctuations in the experimental parameters.

DOI: [10.1103/PhysRevA.86.063404](https://doi.org/10.1103/PhysRevA.86.063404)

PACS number(s): 32.80.Qk, 42.50.Md, 42.50.Gy

**I. INTRODUCTION**

Efficient optical data storage and processing, based on concepts of either classical or quantum computing, are major research topics in optical as well as solid-state physics. Electromagnetically induced transparency (EIT) [1] exhibits a promising approach to realize coherent optical data storage, i.e., optical quantum memories. As prominent applications, EIT permits the deceleration of a light pulse in an optical medium and also the storage of the pulse in an atomic superposition of two quantum states, i.e., an atomic coherence. The atomic coherence contains all relevant information of the light field, i.e., amplitude and phase, and can be restored back into a light pulse on demand. While EIT is a well-established technique in gaseous media (see also [1] and references therein), there are still only a few implementations in solid media. The latter are very attractive for realistic applications of future optical data storage and processing. A specific class of solids, i.e., rare-earth ion-doped crystals, combines the advantages of solids (i.e., large density, scalability, and robustness) and atoms (i.e., spectrally narrow optical transitions and long decoherence times). In the last decade there have been some striking implementations of EIT and optical data storage in rare-earth ion-doped solids [2–5].

However, optical data storage by atomic coherences in doped solids typically suffers from large inhomogeneous broadenings. Upon readout of the memory, this leads to dephasing of the emission from different ensembles of ions prepared in an atomic coherence. Thus, dephasing limits the storage times and storage efficiencies in the retrieved signals. Dephasing provides a general obstacle for atomic coherences, no matter which technique is used to prepare the superposition states (e.g., either EIT with optical pulses or other techniques). We note that in the following we will clearly distinguish between dephasing (i.e., steady phase evolutions, which are due to inhomogeneous broadenings) and decoherence (i.e., statistical phase fluctuations, which are due to homogeneous broadenings). In media with large inhomogeneous broadenings such as rare-earth ion-doped solids, the dephasing time

is typically much shorter than the decoherence time and puts the strongest limits on storage times in atomic coherences. While, in general, it is hard to control decoherence, there are rather straightforward and well-known solutions to cope with dephasing, e.g., the simple and well-established Hahn spin echo [6]. The technique applies an excitation pulse with an area of  $\pi$  to rephase atomic coherences.

Rephasing of spin coherences by  $\pi$  pulses is usually easy to implement, e.g., by radio-frequency (RF) pulses tuned to a magnetic transition between the corresponding states. However, the  $\pi$  pulse must be sufficiently short to cover the spectral bandwidth of the dephasing ensembles. The larger the ensemble bandwidth is, the shorter the required pulse duration is and the larger the required intensity to reach a pulse area of  $\pi$  is. Moreover, fluctuations in the pulse duration, intensity, carrier frequency, or temporal pulse shape modulate the effective pulse area and perturb the rephasing process. Thus, rephasing by  $\pi$  pulses is limited to ensembles with rather small inhomogeneous bandwidth and conditions of sufficiently stable implementation, i.e., without fluctuations of experimental parameters. Such limitations become even more critical if  $\pi$  pulses are applied in complex protocols involving large sequences of rephasing pulses. The latter are required, e.g., for dynamic decoherence control to further prolong storage times [7,8].

In the following, we compare the standard rephasing by  $\pi$  pulses to an alternative approach based on rapid adiabatic passage (RAP). RAP permits complete and robust population transfer between two quantum states. In contrast to  $\pi$  pulses, RAP does not suffer from fluctuations in the experimental parameters, provided some limits are kept in mind. RAP is a well-established tool in nuclear magnetic resonance (see, e.g., [9–12] and references therein) and also permits complete population transfer by optical excitations [13]. As an example of recent research efforts in the field (which are also related to our work), we note the experiments by Lauro *et al.* on rephasing of nuclear spins by RAP in  $\text{Tm}:\text{YAG}$  [14].

In this work we present a systematic comparison of rephasing by  $\pi$  pulses or RAP in order to determine the limitations and advantages of both rephasing techniques, as well as to enable an optimal choice of experimental parameters for efficient and robust rephasing. The investigations place a

\*simon.mieth@physik.tu-darmstadt.de

particular emphasis on rephasing by RAP in EIT-driven doped solids as efficient optical memories. Nevertheless, we note that our conclusions on RAP-based rephasing are also valid for any other application of rephasing (i.e., beyond EIT).

## II. THEORETICAL BACKGROUND

We will now briefly review the relevant features of light storage by EIT, rephasing by  $\pi$  pulses and rephasing by RAP. To discuss EIT, we consider a  $\Lambda$ -type level system of three states,  $|1\rangle$ ,  $|2\rangle$ , and  $|3\rangle$  (see Fig. 1 for the specific coupling scheme of EIT in our doped solid). An intense optical control pulse with electric field  $E_C(t)$  couples states  $|2\rangle$  and  $|3\rangle$ . A weaker optical probe pulse with electric field  $E_P(t)$  couples states  $|1\rangle$  and  $|3\rangle$ . The corresponding Rabi frequencies are  $\Omega_C(t) = \mu_{23}E_C(t)/\hbar$  and  $\Omega_P(t) = \mu_{13}E_P(t)/\hbar$ , with the transition dipole moments  $\mu_{ij}$ . The control pulse drives the medium to a state of EIT, i.e., it becomes transparent for the probe pulse. Moreover, EIT leads to a compression and a deceleration of the probe pulse in the medium. In this case, the system is prepared in the dark dressed state  $|d\rangle = \cos\theta|1\rangle - \sin\theta|2\rangle$ . The mixing angle  $\theta$  is defined by  $\tan\theta = \Omega_P(t)/\Omega_C(t)$ . We now gradually turn the control and probe pulses off while keeping a fixed ratio of Rabi frequencies (i.e., a fixed mixing angle). In this case, the speed of light in the medium for the probe pulse adiabatically approaches zero, i.e., the probe pulse is finally stopped. The probe photons are transferred into a coherent superposition of states  $|1\rangle$  and  $|2\rangle$ , i.e., an atomic coherence  $\rho_{12}$ . This atomic coherence preserves amplitude and phase information. We consider this dynamics as a “write” process of an optical data bit from the probe pulse into the medium as a memory. To retrieve the optical information after an arbitrary storage time  $\Delta t$ , we turn the control pulse on again. In this “read” process, the control pulse beats with the coherence  $\rho_{12}$  and generates a signal pulse, which is an exact copy of the initial probe pulse. Thus, we transferred the optical information back from the atomic coherence into a probe pulse.

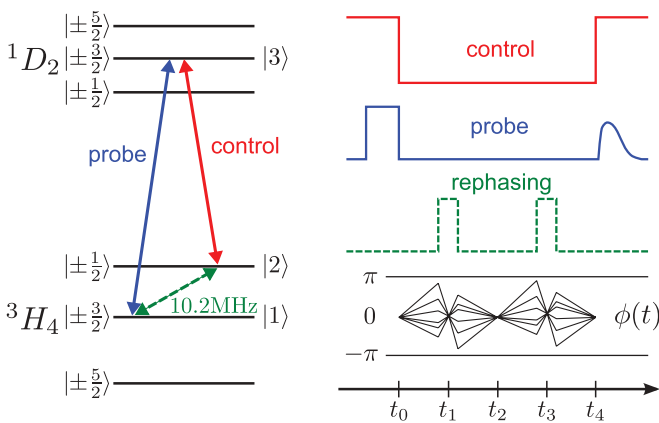


FIG. 1. (Color online) (left) Coupling scheme and relevant hyperfine structure in  $Pr^{3+}:Y_2SiO_5$ . Solid lines indicate optical transitions in EIT. The dashed line indicates the RF transition for rephasing. (right) Schematic overviews of the pulse sequence for light storage combined with RF rephasing pulses and of the phase  $\phi(t)$  in different dopant ensembles.

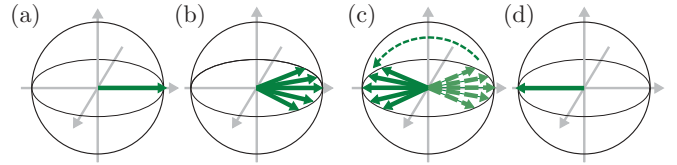


FIG. 2. (Color online) Dephasing and rephasing, depicted on the Bloch sphere. (a) Initial preparation of coherences at time  $t_0$ . (b) Dephasing of four ensembles of coherences ( $t > t_0$ ). (c) A rephasing pulse inverts the phases at  $t_1$ . (d) At time  $t_2$  the four coherences rephase again.

As already briefly discussed in the Introduction, the quantum system (i.e., the optical memory) typically suffers from inhomogeneous broadenings. In the case of doped solids, this is mainly caused by variations of the crystal’s electric field due to lattice imperfections. This leads to variations of the level energies for different ensembles of dopant ions, hence inhomogeneous broadening  $\Gamma_{inh}$  of the transition  $|1\rangle \leftrightarrow |2\rangle$ . Thus, during the EIT write process we prepare a manifold of ensembles oscillating at slightly different atomic coherences  $\rho_{12}^{v_j}$  (where the superscript  $v_j$  indicates a frequency within the inhomogeneous bandwidth). Each ensemble of ions (or the corresponding coherence  $\rho_{12}^{v_j}$ ) yields a different time evolution of the coherence phase  $\phi$ , according to  $\exp[i\phi(t)] = \exp(i2\pi v_j t)$ . Thus, the atomic coherences in different ensembles get out of phase, which leads to destructive interference during the EIT read process. When the storage time exceeds the dephasing time  $T_{dep}$ , the read process will no longer work efficiently.

Figures 2(a)–2(d) and Fig. 1 (right) schematically depict the phase evolution of coherences on the Bloch sphere. When the coherences are initially prepared at time  $t_0$  [see Fig. 2(a)], their phase separation increases with growing time  $t > t_0$ , as indicated in Fig. 2(b). The general strategy to counter dephasing is to drive an inversion of the phase evolution at time  $t_1$  (or an inversion of the population of states  $|1\rangle$  and  $|2\rangle$ , respectively), depicted in Fig. 2(c). The inversion does not affect the direction or the speed of the phase evolution  $\phi(t)$ . Thus, the coherences will rephase again at time  $t_2 = 2t_1$ , but with a total phase change of  $180^\circ$  compared to the initial coherence [see Fig. 2(d)]. To retrieve the initial coherence [see Fig. 2(d)], we require a second inversion process at time  $t_3 = 3t_1$  (see Fig. 1, right). After  $t_4 = 4t_1$  the system is again in its initial state and ready for efficient readout.

A simple way to drive population or phase inversions is the application of  $\pi$  pulses. If we prepare the atomic coherences between spin states (e.g., as in doped solids), this can be implemented by RF pulses with appropriate intensity and duration at the transition between states  $|1\rangle$  and  $|2\rangle$ . We may understand this resonant driving RF field as a torque vector acting on the spins. In the case of  $\pi$  pulses, the torque is perpendicular to the spins and also lies in the equatorial plane of the Bloch sphere. The Rabi frequency  $\Omega_{RF}(t) = \mu_{12}B_{RF}(t)/\hbar$  (with the magnetic transition dipole moment  $\mu_{12}$  and the magnetic field strength  $B_{RF}$ ) must match the condition  $\mathcal{A} = \int \Omega_{RF}(t) dt = \pi$ . This condition is a severe obstacle for the application of  $\pi$  pulses in media of large inhomogeneous bandwidth. At larger bandwidth we require shorter pulses and hence more pulse intensity to obtain a pulse area of  $\pi$ .

Therefore, rephasing of inhomogeneously broadened media by  $\pi$  pulses may become impossible due to limited available pulse intensity. Moreover we note that  $\pi$  pulses are based on diabatic evolution of a quantum system. Thus, any deviation (e.g., due to fluctuations in pulse intensity, temporal shape, duration, or center frequency) from the optimal pulse area of  $\pi$  will lead to less efficient rephasing.

These problems can be overcome by an alternative solution for rephasing, which is based on adiabatic passage. RAP applies a pulse with a frequency chirp around the atomic transition to drive complete population inversion between two quantum states. To rephase an atomic coherence, it is necessary to apply a pair of identical RAP pulses (centered at  $t_1$  and  $t_2$ ). On the Bloch sphere, the RAP torque vector is initially aligned along the population axis, and its direction performs a  $180^\circ$  rotation when the frequency is chirped. The Bloch vector precesses in the equatorial plane around this torque vector. When the frequency detuning  $\Delta(t)$  from the atomic transition is on the order of the Rabi frequency, the Bloch vector flips; i.e., its equatorial angular position is inverted. However, a single RAP process intrinsically induces relative phase shifts depending on the detuning of the corresponding spin transition and Rabi frequency [12]. A second RAP process completes the required phase reversion in all detuned transitions to enable efficient rephasing and to obtain the initial coherence without phase shift.

Efficient implementation of RAP imposes some constraints on the frequency chirp and the Rabi frequency; i.e., we must fulfill the adiabaticity criterion [10,13]. In a simplified version, the adiabaticity criterion for RAP reads  $\Omega_{\text{RF}}^2/R \gg 1$ , with the chirp rate  $R = 2\pi d[\Delta(t)]/dt$ . Moreover, the total chirp range  $\Delta\nu = \int R(t)/(2\pi)dt$  must exceed the Rabi frequency, i.e.,  $2\pi\Delta\nu \gg \Omega_{\text{RF}}$ . The simplified version of the adiabaticity criterion is valid for smooth temporal variations of Rabi frequency and chirp. The condition ensures a full  $180^\circ$  rotation of the Bloch vector on the Bloch sphere. We note that these constraints are rather “soft”. RAP will always work efficiently as long as we operate in between some very coarse limits of Rabi frequency, chirp range, and chirp rate (e.g., irrespective of the exact pulse intensity, temporal shape, or center frequency). Thus, as an adiabatic process RAP suffers far less from fluctuations in the experimental parameters compared to  $\pi$  pulses. Moreover, RAP automatically covers the full inhomogeneous manifold in the medium without the need to increase the pulse intensity, provided the frequency chirp range is larger than the inhomogeneous bandwidth.

We note that all previous work on rephasing of atomic coherences (whether driven optically or by other means) does surprisingly not yet indicate a preference of experimentalists for RAP rather than  $\pi$  pulses. However, from previous work in NMR [9–12] and the above considerations we clearly deduce the following expectations: For media with large inhomogeneous broadenings, implementations with limited control of experimental parameters, or integration in complex pulse sequences we expect RAP to offer significant advantages with regard to rephasing efficiencies. For media with moderate inhomogeneous broadenings and/or sufficient control of experimental parameters, we expect both techniques to provide similar efficiency, although  $\pi$  pulses are simpler to implement. In the following we will systematically compare

rephasing by  $\pi$  pulses or RAP in order to confirm, modify, or specify these expectations, and we provide advice for particular experimental conditions.

### III. EXPERIMENTAL SETUP

We perform the experiments in a  $\text{Pr}^{3+}:\text{Y}_2\text{SiO}_5$  crystal (hereafter termed PrYSO) with a dopant concentration of 0.05%. If not indicated otherwise, the crystal has a length of  $L = 3$  mm, yielding an optical depth of  $\alpha L \approx 4$ . The crystal is placed inside a liquid helium cryostat (Janis Research ST-100), yielding temperatures of 4 K for the sample. Figure 1 (left) shows the relevant hyperfine structure of  $\text{Pr}^{3+}$  ions in the host lattice. The optical probe field couples the transition between states  $|1\rangle = |^3H_4, m_I = \pm\frac{3}{2}\rangle$  and  $|3\rangle = |^1D_2, m_I = \pm\frac{3}{2}\rangle$ . The optical control field couples the transition between states  $|2\rangle = |^3H_4, m_I = \pm\frac{1}{2}\rangle$  and  $|3\rangle$ . The rephasing pulses couple the RF transition between  $|1\rangle$  and  $|2\rangle$  at a frequency  $\nu_{\text{RF}} = 10.2$  MHz. The lifetime of these hyperfine states is  $T_1 = 100$  s. The inhomogeneous bandwidth of the RF transition is  $\Gamma_{\text{inh}} \approx 30$  kHz [15]. This corresponds to a dephasing time in the range of  $T_{\text{dep}} = 1/(\pi\Gamma_{\text{inh}}) \approx 10$   $\mu\text{s}$  [16]. Without rephasing, the dephasing time also limits the maximal storage time in atomic coherences. With rephasing, the maximal storage time can approach the decoherence time of the RF transition, which is about 500  $\mu\text{s}$  [17].

The laser radiation at wavelengths around  $\lambda = 605.98$  nm is provided by a single longitudinal mode dye laser (SIRAH Matisse-DX) with a linewidth of 100 kHz. The radiation is split into a stronger control beam ( $P_C \approx 100$  mW) and a weaker probe beam ( $P_P \approx 4$  mW). The beams are guided through acousto-optical modulators in a double-pass configuration, which allow for full control of temporal intensity and frequency profiles. The control and probe beams are mildly focused and intersect in the crystal. The beam diameters (full width at half maximum) are  $d_C = 220$   $\mu\text{m}$  and  $d_P = 150$   $\mu\text{m}$ . This yields peak Rabi frequencies of  $\Omega_C = 2\pi \times 950$  kHz and  $\Omega_P = 2\pi \times 280$  kHz, respectively. The duration of the stored probe pulse is 20  $\mu\text{s}$ . A pair of coils in Helmholtz configuration, placed around the crystal inside the cryostat, serves to introduce RF pulses. The RF pulses are generated by an arbitrary waveform generator (Tektronix AWG 5014) and are amplified by a power amplifier (EM Power 1028-BBM 1C3KAJ) with a maximal output power of 10 W. To optimize power transmission between amplifier and RF coils, we use a single-frequency impedance matching circuit (3 dB bandwidth, 600 kHz). In the experiments we apply RF pulses with (if not indicated otherwise) rectangular temporal profile and pulse durations below 100  $\mu\text{s}$ . For rephasing by RAP, we induce linear frequency chirps around the center frequency  $\nu_C$  in the range of  $\Delta\nu = 50$ –900 kHz. The RF setup enables Rabi frequencies up to  $\Omega_{\text{RF}} \approx 2\pi \times 140$  kHz. We note that even for a bandwidth of 600 kHz, also at frequencies of  $\nu = \nu_C \pm 450$  kHz the RF matching circuit allows Rabi frequencies of more than  $\Omega_{\text{max}}/2$ . Even for large chirp ranges, the rectangular pulses still exhibit quite steep rising and falling edges, although they do not provide a perfect flat top profile.

We also note that prior to the experiment on light storage and rephasing we prepare the doped solid by optical pumping to

create a spectrally isolated  $\Lambda$  system. For a detailed description of this preparation sequence we refer the reader to [16,18].

Figure 1 (right) schematically depicts the relevant pulse sequences for light storage and rephasing (after the preparation sequence). The control and probe pulses generate a coherent superposition of states  $|1\rangle$  and  $|2\rangle$ . We choose a storage time of  $\Delta t = 600 \mu\text{s}$  (i.e., in the range of the decoherence time, but well above the dephasing time) before reading out the coherence with a second control pulse to retrieve the probe pulse. During the storage time  $\Delta t$  we apply two rephasing pulses (either  $\pi$  or RAP pulses) at  $t_1 = 150 \mu\text{s}$  and  $t_3 = 3t_1 = 450 \mu\text{s}$ . In all measurements we keep the experimental parameters for the light storage and retrieval sequence (i.e., the control and probe pulses) fixed, while we systematically vary the parameters in the rephasing sequence. We determine the performance of the rephasing processes by monitoring the power of the retrieved probe pulse on a photodiode (Newfocus Model 2051). Integration of this signal yields the retrieved probe pulse energy, which is directly proportional to the retrieval efficiency and hence the rephasing efficiency.

#### IV. EXPERIMENTAL RESULTS

In the experiment we now apply either  $\pi$  or RAP pulses to rephase the EIT-driven coherences. We compare the energy of the retrieved probe pulse (i.e., the retrieval efficiency) for the two rephasing strategies, also considering the dependence upon systematic variations of the experimental parameters. In a first measurement, we determine the dependence of the retrieved probe pulse energy vs the Rabi frequency  $\Omega_{\text{RF}}$  (or the available RF power) for both  $\pi$  and RAP rephasing pulses. To enable a fair comparison of both techniques vs the Rabi frequency, we proceed as follows: For any fixed Rabi frequency  $\Omega_{\text{RF}}$  we choose the pulse duration of the rephasing  $\pi$  pulses such that we reach a maximum in the retrieved probe pulse energy. In the same way, for any fixed Rabi frequency  $\Omega_{\text{RF}}$  we choose the pulse duration and the chirp rate of the rephasing RAP pulses such that we reach a maximum in the retrieved probe pulse energy with the shortest possible pulse.

We use rectangular pulses both for rephasing by  $\pi$  pulses and for RAP rephasing. Short rectangular pulses are the best choice for rephasing of inhomogeneously broadened media by  $\pi$  pulses, as the pulse spectrum is broad. For RAP rephasing, smoother temporal shapes and longer pulse durations would be better due to the constraints of adiabaticity. Thus, rectangular pulse shapes in a RAP sequence yield some residual oscillations of the retrieval efficiency vs pulse duration (for details, see also discussion of Fig. 6). We choose the RAP pulse duration to obtain maximal rephasing efficiency with the shortest possible pulse. This is a very favorable situation for  $\pi$  pulses, although not yet optimal for RAP, as we operate at the edge of the adiabaticity criterion. However, it enables a (more than) fair comparison with  $\pi$  pulses. Nevertheless, even under the less favorable conditions, RAP already yields a large efficiency and superior performance compared to rephasing by  $\pi$  pulses, as we will shortly see.

We also note that the application of rather short and comparable pulse durations involves another aspect for a fair comparison of the rephasing strategies: When we apply comparable durations of RAP and  $\pi$  pulses, the flipping time

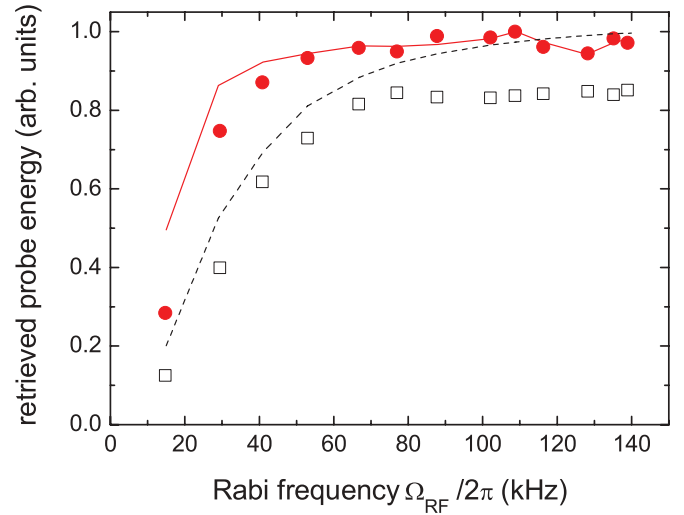


FIG. 3. (Color online) Retrieved probe pulse energy vs Rabi frequency  $\Omega_{\text{RF}}$ , either for rephasing with  $\pi$  pulses (black open squares) or RAP pulses (red solid circles). The duration of the optimized  $\pi$  pulses varies from 34 to 3.6  $\mu\text{s}$ . The duration of the optimized RAP pulses duration varies from 75 to 6.5  $\mu\text{s}$ , and the chirp range varies from  $\Delta\nu = 50 \text{ kHz}$  to  $\Delta\nu = 600 \text{ kHz}$ . The red solid line and the black dashed line show numerical simulations for rephasing by RAP and  $\pi$  pulses, respectively.

of the rephasing process is usually shorter in the case of a RAP pulse. During the flipping time, i.e., when the detuning  $\Delta(t)$  is in the range of  $\Omega_{\text{RF}}$ , the spins have a non-negligible component on the population axis in the Bloch sphere. Therefore, the spins decay not only with the decoherence time  $T_2 = 500 \mu\text{s}$  but also with the population life time  $T_1 = 100 \text{ s}$ . A longer flipping time would result in higher rephasing efficiency as a  $T_1$  decay is much slower compared to a  $T_2$  decay. Thus, for the comparison between  $\pi$  and RAP pulses we keep the similar (and rather short) pulse durations for rephasing  $\pi$  pulses and RAP pulses so as not to provide any unfair advantage for RAP.

Figure 3 shows the results of the comparison between RAP and  $\pi$  pulses as well as numerical simulations for the measurements, i.e., the retrieved probe pulse energy vs Rabi frequency. The black open squares (black dashed line for the simulation) depict the data after rephasing with  $\pi$  pulses, and the red solid circles (and red solid line for the corresponding simulation) depict the data after rephasing with RAP pulses. See also Table I to find the exact pulse parameters for every data point and the simulation. Let us first consider the experimental data. Obviously, in both strategies, the retrieved probe energy increases with increasing Rabi frequency. In the case of  $\pi$  pulses this is because at larger Rabi frequency the optimal pulse duration is shorter. Hence the spectral bandwidth increases and covers a larger part of the inhomogeneous manifold in the medium. In the case of RAP at larger Rabi frequencies we are able to apply larger chirp ranges without substantially decreasing  $\Omega_{\text{RF}}^2/R$  in the optimal case (see also Table I). Hence we better fulfill the condition  $2\pi\Delta\nu \gg \Omega_{\text{RF}}$  (see above) and also drive a larger part of the inhomogeneous manifold in a fully adiabatic and therefore more efficient way. As the data clearly indicate, rephasing by RAP is superior to rephasing by  $\pi$  pulses for all Rabi frequencies. As expected, the frequency

TABLE I. Experimental parameters for rephasing by  $\pi$  pulses and RAP, as relevant to the single data points and simulations in Fig. 3.  $\Omega_{\text{RF}}$  is the Rabi frequency,  $\tau_{\pi}$  and  $\tau_{\text{RAP}}$  are pulse durations of  $\pi$  and RAP pulses, and  $\Delta\nu$  is the chirp range. The inhomogeneous broadening used for the simulation is  $\Gamma_{\text{inh}} = 44$  kHz.

$\Omega_{\text{RF}} (2\pi \text{ kHz})$	$\tau_{\pi} (\mu\text{s})$	$\tau_{\text{RAP}} (\mu\text{s})$	$\Delta\nu (\text{kHz})$	$\frac{\Omega_{\text{RF}}^2}{R}$	$\frac{2\pi\Delta\nu}{\Omega_{\text{RF}}}$
140	3.6	6.5	600	1.33	4.29
135	3.7	7	600	1.34	4.45
128	3.9	6.5	600	1.12	4.69
116	4.3	7.5	500	1.27	4.31
109	4.6	9	400	1.68	3.67
102	4.9	9	400	1.47	3.92
88	5.7	10.1	350	1.40	3.98
77	6.5	11.5	300	1.43	3.90
67	7.5	14	250	1.58	3.73
53	9.45	16.5	200	1.46	3.77
41	12.25	24	150	1.69	3.66
29	17	36.5	100	1.93	3.45
15	34	75	50	2.12	3.33

chirp in RAP enables us to rephase the full inhomogeneous manifold at high RF power. For lower, i.e., limited, RF power, RAP pulses still yield a relatively high rephasing efficiency. In comparison, the rephasing bandwidth by  $\pi$  pulses is limited by the available RF power. In particular for lower Rabi frequencies, this becomes an obstacle for rephasing by  $\pi$  pulses. Thus, the relative enhancement of RAP compared to  $\pi$  rephasing ranges between a factor of 1.15 for larger Rabi frequencies (i.e., RF powers) and more than a factor of 2 for small Rabi frequencies. We note that the effect of different flipping times in RAP and  $\pi$  pulse rephasing yields only enhancements of 1.004 (for large Rabi frequencies) and 1.15 (for small Rabi frequencies) in the efficiency. Thus, the effect is negligible.

The numerical simulations in Fig. 3 confirm the experimental data. The simulation involves the parameters shown in Table I. We note that, in addition the experimental data, the simulation is also normalized to its maximum. Hence, we do not compare absolute values, but the relative changes caused by inhomogeneous broadening. Our above arguments for the change of rephasing efficiencies are well confirmed by the simulation. However, according to the simulation, for large Rabi frequencies the rephasing efficiency for  $\pi$ -pulse-based rephasing should approach the efficiency for RAP-based rephasing.

We note that Fig. 3 indicates an optimal performance of  $\pi$  pulses for Rabi frequencies beyond  $\Omega_{\text{RF}} \approx 2\pi \times 60$  kHz. The corresponding frequency bandwidth of the (rectangular shaped)  $\pi$  pulse is 60 kHz ( $\tau_{\pi} = 7.5 \mu\text{s}$ ) and is obviously larger than the inhomogeneous bandwidth of about 30 kHz in the medium. Thus, we would expect efficient rephasing of the full inhomogeneous manifold by  $\pi$  pulses beyond  $\Omega_{\text{RF}} \approx 2\pi \times 60$  kHz, just as predicted by the simulation. We would not expect to observe a better performance by RAP at these larger Rabi frequencies (which the data nevertheless indicate). Thus, rephasing of the doped solid by  $\pi$  pulses seems to suffer from additional problems at larger RF powers, which do not affect rephasing by RAP. As we will discuss in more detail below, this perturbing effect is due to spatial inhomogeneities of the magnetic RF field in the interaction

region, i.e., the PrYSO crystal. Such problems are well known also in NMR applications of  $\pi$  pulses (see [10] and references therein). Although in the center of perfect RF coils the driving RF field should be homogeneous, the field strength and direction slightly vary outside the center of the coils. This becomes even worse if we consider a less perfect coil geometry. As the interaction region has a spatial extension, in the experiment we average over spatially slightly varying RF Rabi frequencies. This variation of experimental parameters reduces the performance of rephasing by  $\pi$  pulses, which require exact choice and maintenance of the field strength and pulse duration over whole the interaction region. Such variations of experimental parameters are no problem for the robust RAP process, which still operates at maximal efficiency.

The different effect of field inhomogeneities upon the two rephasing strategies becomes very obvious when we work with a larger interaction region, e.g., when we apply a longer PrYSO crystal. Thus, we perform the experiments in two PrYSO crystals of different lengths, i.e., a short crystal of  $L = 1$  mm and a longer PrYSO crystal of  $L = 10$  mm ( $\alpha \times 1 \text{ mm} \approx 1.3$ ,  $\alpha \times 10 \text{ mm} \approx 13$ , but otherwise they have the same specifications). Due to the larger extension of the interaction region, we must average over larger RF field inhomogeneities, which will more strongly affect rephasing in our experiment. To compare the performance of rephasing by  $\pi$  and RAP under these conditions, we choose a Rabi frequency of  $\Omega_{\text{RF}} \approx 2\pi \times 70$  kHz and optimize the parameters of the  $\pi$  and RAP pulses (i.e., pulse durations and chirp range) to obtain maximal retrieval efficiency in both cases. We note (see Fig. 3) that operation at this sufficiently large Rabi frequency provides the best possible conditions for rephasing by  $\pi$  pulses. Figure 4(a) shows the temporal profiles of retrieved probe pulses from the short PrYSO crystal for rephasing either by  $\pi$  or RAP pulses. In the short crystal RAP pulses provide a factor of 1.15 larger retrieval efficiency compared to  $\pi$  pulses. In the longer crystal, rephasing by  $\pi$  pulses suffers much more from RF field inhomogeneities and yields a much worse retrieval efficiency. Rephasing by RAP is not affected by the inhomogeneities. Thus, in the long crystal RAP rephasing even yields a factor of 1.67 more retrieved pulse energy compared to  $\pi$  pulses [see Fig. 4(b)]. The different temporal shapes of the retrieved light pulses are due to pulse propagation effects in the two crystal samples with different lengths. However, for the interpretation of the data in Fig. 4 with regard to a comparison of the rephasing strategies this is of no particular interest.

We further confirm now experimentally the robustness of RAP rephasing with regard to variations in the driving RF field. In the setup we apply again the PrYSO crystal with 3 mm length. We optimized the  $\pi$  and RAP pulses for rephasing at a large Rabi frequency of  $\Omega_{\text{RF}} = 2\pi \times 140$  kHz, corresponding to the maximal RF power  $P = 10$  W in our setup. As discussed above, operation at a large Rabi frequency (hence small pulse duration and large spectral bandwidth) provides the optimal conditions for rephasing of the inhomogeneous manifold by  $\pi$  pulses. The pulse duration of the optimized  $\pi$  pulse is  $\tau_{\pi} = 3.5 \mu\text{s}$ . The pulse duration of the optimized RAP pulse is  $\tau_{\text{RAP}} = 51 \mu\text{s}$ , and the chirp range  $\Delta\nu = 600$  kHz. Starting from these pulses, we now reduce the Rabi frequency (while keeping the pulse durations and chirp range fixed)

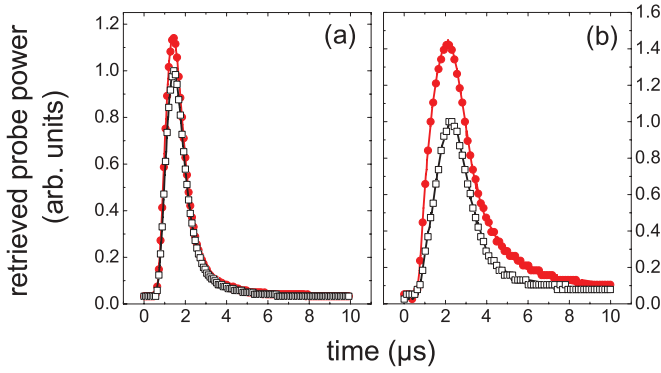


FIG. 4. (Color online) Temporal pulse shapes for retrieved probe pulses from a PrYSO crystal with a length of (a) 1 or (b) 10 mm for rephasing by  $\pi$  pulses (black open squares) or RAP pulses (red solid circles).

and monitor the variation of the retrieved probe pulse energy vs Rabi frequency. This mirrors an experimental situation, which suffers from variations of the Rabi frequency (or the RF power). Figure 5 shows the results of this measurement. We note that in Fig. 5 we do not compare the *absolute* values of the retrieval efficiency for the two strategies, but their relative change with the Rabi frequency. RAP yields a large retrieval efficiency over a wide range of Rabi frequencies beyond  $\Omega_{\text{RF}} = 2\pi \times 70$  kHz. For the corresponding experimental parameters the adiabaticity criterion yields  $\Omega_{\text{RF}}^2/R > 2.6$ ; i.e., we approach the condition for adiabatic evolution  $\Omega_{\text{RF}}^2/R \gg 1$ . Thus, the performance of rephasing by RAP does not suffer from variations in the Rabi frequency, provided we operate with Rabi frequencies above  $2\pi \times 70$  kHz. In the case of rephasing by  $\pi$  pulses, the variation of the Rabi frequency exhibits a severe problem: As the data show, the performance of  $\pi$  pulses decreases quickly for decreasing

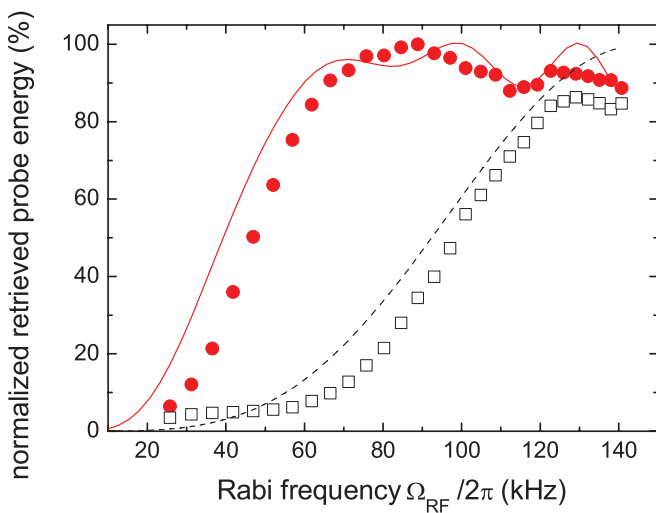


FIG. 5. (Color online) Normalized retrieved probe pulse energy vs Rabi frequency for  $\pi$  pulses and RAP pulses with fixed pulse durations and chirp range. Data for  $\pi$  pulses are set as black open squares. Data for RAP pulses are set as red solid circles. The red solid line and the black dashed line show numerical simulations for rephasing by RAP and  $\pi$  pulses, respectively.

Rabi frequency. The region of efficient rephasing by  $\pi$  pulses is much smaller compared to RAP. Moreover, rephasing by  $\pi$  pulses completely starts to fail for Rabi frequencies below  $2\pi \times 60$  kHz, while rephasing by RAP still permits efficient retrieval.

Figure 5 also shows numerical simulations for rephasing by RAP (red solid line) and  $\pi$  pulses (black dashed line). The simulations are in good agreement with the measured data. Small deviations between simulations and experimental data (e.g., for large Rabi frequencies in  $\pi$  pulse rephasing) are due to imperfections and perturbations (e.g., inhomogeneities in the RF fields), which are not taken into account in the simulations. However, it becomes very clear that rephasing by RAP offers enhanced robustness and efficiency compared to rephasing by  $\pi$  pulses. This holds particularly true when we deal with realistic (i.e., less perfect or stable) experimental conditions and in inhomogeneously broadened media.

In the following, we provide some comments on the design of optimal RAP rephasing pulses, e.g., for applications of light storage by EIT. As already discussed above, we must consider and fulfill the adiabaticity criterion for RAP; i.e., we must provide sufficiently large Rabi frequency and chirp range. We also note that in contrast to diabatic processes (e.g.,  $\pi$  pulses) adiabatic excitations require sufficiently smooth pulse envelopes in time. Thus, for optimal operation the RAP pulses must not exhibit too fast temporal variations, e.g., intensity spikes or very steep rising and falling edges. However, the latter condition is not too critical, provided some limits are kept in mind. Indeed, in the above experiments we applied RAP pulses with rectangular temporal pulse envelopes. Already for this less than perfect situation, RAP always showed much better performance compared to  $\pi$  pulses. If we apply smooth (e.g., Gaussian shaped) pulse envelopes, the performance of RAP becomes even better.

Figure 6 shows a comparison of the retrieved probe pulse energy (i.e., rephasing efficiency) by RAP for different temporal pulse profiles, i.e., rectangular or Gaussian envelopes. For all data points we keep the Rabi frequency  $\Omega_{\text{RF}} \approx 2\pi \times 135$  kHz fixed while varying the pulse duration. We note that varying the pulse duration while keeping the chirp range fixed also automatically changes the chirp rate. Let us first consider RAP pulses with rectangular pulse shape and a fixed chirp range  $\Delta\nu = 600$  kHz (depicted by black open squares in Fig. 6). For small pulse durations, we do not fulfill the adiabaticity criterion, e.g., the chirp rate is too large for the fixed Rabi frequency. For increasing pulse duration, we fulfill the adiabaticity criterion better. Thus, rephasing by RAP works better and approaches a first maximum at a pulse duration around 6–7  $\mu\text{s}$ . However, a further increase in the pulse duration yields pronounced oscillations of the retrieved pulse energy. Such oscillations are a typical feature of residual diabatic couplings. Perfectly adiabatic processes (such as RAP) should not show oscillatory behavior. Two well-known phenomena contribute to this behavior: First, rectangular pulses exhibit steep intensity changes in the rising and falling edges. Thus, the excitation dynamics is not perfectly adiabatic all over the pulse, and residual diabatic interactions occur [19]. Second, an insufficient fulfillment of the condition  $2\pi \Delta\nu / \Omega_{\text{RF}} = 4.4$  (for our experimental parameters) also leads to residual diabatic behavior [9,10].

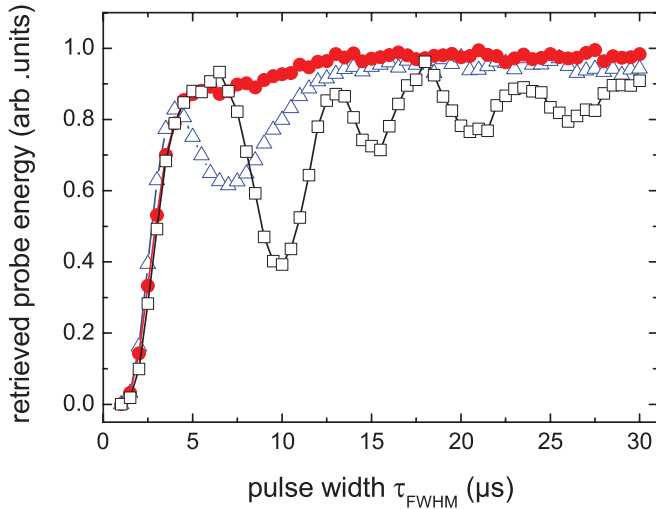


FIG. 6. (Color online) Retrieved probe pulse energy after rephasing by RAP pulses vs pulse width for driving RF pulses of different temporal shape. We apply either rectangular pulses and a chirp range  $\Delta\nu = 600$  kHz (black open squares) or Gaussian pulses and a chirp range of  $\Delta\nu = 600$  kHz (blue open triangles) or Gaussian pulses and a chirp range of  $\Delta\nu = 900$  kHz (red solid circles). The Rabi frequency is kept constant at  $\Omega_{RF} \approx 2\pi \times 135$  kHz for all data points.

To reduce diabatic couplings, we now consider RAP pulses with a Gaussian envelope (depicted by blue open triangles in Fig. 6), i.e., a change in the pulse shape. The maximum amplitude of the Gaussian pulse is given by the Rabi frequency  $\Omega_{RF}$ . For all measurements with Gaussian-shaped pulses we set the pulse width as full width at half maximum  $\tau_{FWHM} = 2\sigma\sqrt{2\ln 2}$  (with the standard deviation  $\sigma$ ) and define the total pulse duration by 3 times  $\tau_{FWHM}$ . Hence, the pulse is truncated symmetrically at  $\pm 3/2\tau_{FWHM}$  around its maximum; i.e., it starts with below 0.2% of its maximum amplitude. This choice also yields equivalent pulse areas for both pulse shapes at equal pulse width. For pulses with a Gaussian temporal profile, the retrieval efficiency does not show many oscillations any longer. Instead, we observe an almost-constant plateau of large retrieval efficiency for longer pulse durations. The plateau reveals smooth, robust, adiabatic evolution.

Nevertheless, we still get some residual diabatic behavior for Gaussian pulses at small pulse durations, yielding a pronounced single oscillation around pulse durations of 5–10  $\mu\text{s}$ . If we additionally increase the chirp range and thereby  $2\pi\Delta\nu/\Omega_{RF}$  by a factor of 1.5, we obtain a perfect adiabatic evolution in RAP rephasing (see Fig. 6, red solid circles).

To further investigate the influence of pulse shape and chirp range upon the oscillatory behavior, we performed numerical simulations. Figure 7 shows calculated rephasing efficiencies vs pulse duration for different chirp ranges in a RAP sequence with rectangular pulse shapes. For comparison with experimental data, the black open squares indicate the measured results from Fig. 6 (i.e., for a rectangular pulse shape and a chirp range of 600 kHz). The black solid line shows the corresponding simulation. The simulation fits very well with the data. We now increase the chirp range (and thereby the chirp rate) by a factor of 1.5 while maintaining all other parameters (i.e., the same as in the experiment).

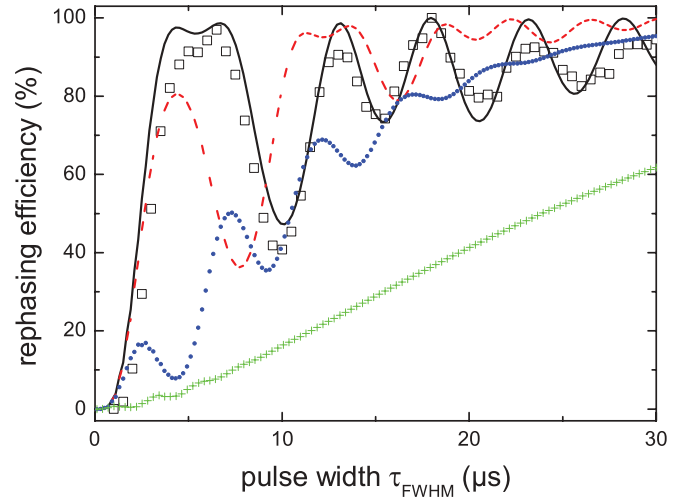


FIG. 7. (Color online) Simulation of rephasing efficiency vs pulse width of rectangular-shaped RAP pulses with different chirp ranges. The black open squares represent normalized experimental data with chirp range  $\Delta\nu = 600$  kHz. The black solid line shows a simulation matched to the experimental data. The red dashed line depicts a simulation with 1.5 times the original chirp range, the blue dots show a simulation with 3 times the original chirp range, and the green crosses represent a simulation with 6.5 times the original chirp range.

The calculated rephasing efficiency vs pulse duration for the larger chirp rate is depicted in Fig. 7 by the red dashed line. The simulation shows a damping of the oscillations, but nevertheless, they do not disappear as in the case of a Gaussian pulse shape. Moreover, the calculation shows a decrease of the rephasing efficiency for short pulse durations. This is because the ratio  $\Omega_{RF}^2/R$  (i.e., the adiabaticity) decreases with increasing chirp rate. For even larger chirp rate (i.e., thrice the initial value), the trend continues. Finally, the oscillation almost completely disappears for a chirp range 6.5 times larger than the initial value (depicted by the green crosses in Fig. 7), i.e.,  $2\pi\Delta\nu/\Omega_{RF} = 28.9$ . However, the rephasing efficiency is poor. We must note that due to the large chirp range the initial relative amplitude of the effective Rabi frequency, given by  $(\Omega_{RF}/\Omega_{eff})^2 = \Omega_{RF}^2/[\Omega_{RF}^2 + [\Delta(t=0)/2]^2]$ , is very low; i.e., a large chirp range compensates a steep falling or rising edge at the beginning and the end of the pulse. In the case of a Gaussian-shaped RAP pulse (see Fig. 6, solid red circles), we only get  $2\pi\Delta\nu/\Omega_{RF} = 6.7$ . However, no diabatic oscillations occur, and the retrieval efficiency is large, even at short pulse durations. A comparison of the experimental data in Fig. 6 (which indicate the variation of the performance of RAP with different pulse shapes) with the numerical simulations in Fig. 7 (which indicate the effect of the chirp range upon the RAP performance) shows that both temporal pulse shape and chirp range affect residual oscillations in the retrieval efficiency. Indeed, the chirp range also enters in the adiabaticity criterion  $\Omega_{RF}^2/R$ , which intrinsically also involves the pulse duration. Under realistic experimental conditions all of these parameters are limited, which also limits the range of adiabatic operation. On the other hand, appropriate pulse shapes permit a quite strong suppression of residual diabatic couplings (as confirmed by the experimental data in Fig. 6) without critically affecting the adiabaticity criterion.

## V. CONCLUSION

We presented a systematic investigation of rapid adiabatic passage, applied to rephasing optically driven atomic coherences in a solid memory, i.e., a  $\text{Pr}^{3+}:\text{Y}_2\text{SiO}_5$  crystal. We compared the performance of RAP with the well-established Hahn spin echo (also termed  $\pi$  pulses). In particular, we studied the retrieval efficiency of light pulses stored in an atomic coherence, driven by electromagnetically induced transparency. While we write and read the coherence optically, the rephasing RAP or  $\pi$  pulses are implemented by magnetic RF sequences. In the first experiment we compared rephasing of coherences by RAP or  $\pi$  pulses when varying the Rabi frequency (or the driving RF power). Rephasing by RAP permitted an enhancement of the retrieval efficiency in light storage by up to a factor of 2 compared to  $\pi$  pulses. This is mainly because large inhomogeneous broadenings in the solid medium require very short and intense  $\pi$  pulses to cover the inhomogeneous linewidth by the pulse bandwidth. RAP permits coverage of the inhomogeneous linewidth simply by a frequency chirp, without the need for short pulse durations and larger driving RF power. In the second experiment, we investigated the effect of inhomogeneities in the driving RF field upon rephasing. RAP proved to be much more robust compared to rephasing by  $\pi$  pulses. Thus, RAP also yielded significantly enhanced retrieval efficiencies in light storage under conditions of larger field inhomogeneities. The robustness of RAP was also demonstrated in the third experiment, which dealt with the effect of variations and fluctuations in the driving RF power (or Rabi frequency). Here,

RAP proved to permit stable rephasing of atomic coherences in a much larger range of Rabi frequencies compared to  $\pi$  pulses. Finally, in the fourth experiment we showed that pulses of smooth temporal profile (e.g., Gaussian pulse envelopes) offer perfect conditions for most robust and efficient rephasing by RAP, although rectangular pulses also already work well. In summary, our experimental investigations clearly demonstrate the advantages of rephasing by RAP compared to the well-established  $\pi$  pulses. In contrast to  $\pi$  pulses, rephasing by RAP does not suffer from inevitable fluctuations of experimental parameters or inhomogeneous broadenings in the optical memory, provided some limits are kept in mind. RAP combines a large efficiency with pronounced robustness. Thus, RAP exhibits a robust tool to prolong storage times and enhance storage efficiencies, e.g., for applications of light storage by EIT (and any other protocol involving broadband rephasing) in solid media with large inhomogeneous bandwidth.

## ACKNOWLEDGMENTS

The authors acknowledge valuable comments and experimental support by G. Heinze (TU Darmstadt), as well as discussions with M. F. P. Winter and T. Chanelière (CNRS, Orsay). The research leading to these results has received funding from the Deutsche Forschungsgemeinschaft, the Volkswagen Foundation, and the People Programme (Marie Curie Actions) of the European Union's Seventh Framework Programme FP7/2007-2013/ under REA Grant No. 287252.

- 
- [1] M. Fleischhauer, A. Imamoglu, and J. P. Marangos, *Rev. Mod. Phys.* **77**, 633 (2005).
  - [2] A. V. Turukhin, V. S. Sudarshanam, M. S. Shahriar, J. A. Musser, B. S. Ham, and P. R. Hemmer, *Phys. Rev. Lett.* **88**, 023602 (2001).
  - [3] J. J. Longdell, E. Fraval, M. J. Sellars, and N. B. Manson, *Phys. Rev. Lett.* **95**, 063601 (2005).
  - [4] B. S. Ham, M. S. Shahriar, and P. R. Hemmer, *Opt. Lett.* **22**, 1138 (1997).
  - [5] G. Heinze, A. Rudolf, F. Beil, and T. Halfmann, *Phys. Rev. A* **81**, 011401(R) (2010).
  - [6] E. L. Hahn, *Phys. Rev.* **80**, 580 (1950).
  - [7] L. Viola, E. Knill, and S. Lloyd, *Phys. Rev. Lett.* **82**, 2417 (1999).
  - [8] W. Yang, Z.-Y. Wang, and R.-B. Liu, *Front. Phys.* **6**, 2 (2011).
  - [9] C. J. Hardy, W. A. Edelstein, D. Vatis, R. Harms, and W. J. Adams, *Magn. Reson. Imaging* **3**, 107 (1985).
  - [10] M. Garwood and L. DelaBarre, *J. Magn. Reson.* **153**, 155 (2001).
  - [11] R. A. De Graaf and K. Nicolay, *Concepts Magn. Reson.* **9**, 247 (1997).
  - [12] S. Conolly, G. Glover, D. Nishimura, and A. Macovski, *Magn. Reson. Med.* **18**, 28 (1991).
  - [13] N. V. Vitanov, T. Halfmann, B. W. Shore, and K. Bergmann, *Annu. Rev. Phys. Chem.* **52**, 763 (2001).
  - [14] R. Lauro, T. Chanelière, and J.-L. Le Gouët, *Phys. Rev. B* **83**, 035124 (2011).
  - [15] K. Holliday, M. Croci, E. Vauthey, and U. P. Wild, *Phys. Rev. B* **47**, 14741 (1993).
  - [16] F. Beil, J. Klein, G. Nikoghosyan, and T. Halfmann, *J. Phys. B* **41**, 074001 (2008).
  - [17] B. S. Ham, M. S. Shahriar, M. K. Kim, and P. R. Hemmer, *Opt. Lett.* **22**, 1849 (1997).
  - [18] M. Nilsson, L. Rippe, S. Kröll, R. Klieber, and D. Suter, *Phys. Rev. B* **70**, 214116 (2004).
  - [19] N. V. Vitanov, *Phys. Rev. A* **59**, 988 (1999).